# Detailed study of nuclear fusion from femtosecond laser-driven explosions of deuterium clusters

J. Zweiback,[a] T. E. Cowan,[a] J. H. Hartley, R. Howell, K. B. Wharton,[b] J. K. Crane, V. P. Yanovsky,[c] and G. Hays
*Lawrence Livermore National Laboratory, L-477, Livermore, California 94550*

R. A. Smith
*Imperial College of Science Technology and Medicine, London SW7 2BZ, United Kingdom*

T. Ditmire
*Lawrence Livermore National Laboratory, L-477, Livermore, California 94550 and Department of Physics, University of Texas, Austin, Texas 78712*

(Received 26 November 2001; accepted 25 April 2002)

Recent experiments on the interaction of intense, ultrafast pulses with large van der Waals bonded clusters have shown that these clusters can explode with sufficient kinetic energy to drive nuclear fusion. Irradiating deuterium clusters with a 35 fs laser pulse, it is found that the fusion neutron yield is strongly dependent on such factors as cluster size, laser focal geometry, and deuterium gas jet parameters. Neutron yield is shown to be limited by laser propagation effects as the pulse traverses the gas plume. From the experiments it is possible to get a detailed understanding of how the laser deposits its energy and heats the deuterium cluster plasma. The experiments are compared with simulations. © *2002 American Institute of Physics.* [DOI: 10.1063/1.1487382]

## I. INTRODUCTION

A number of experiments have been conducted in recent years examining the interactions of intense femtosecond laser pulses with large van der Waals bonded clusters.[1–15] These experiments have been accompanied by a range of theoretical models.[4,16–23] Most of this work has shown that these interactions can be very energetic, with a variety of experimental manifestations. Very bright x-ray emissions in the 100–5000 eV range have been observed;[2,3,8,15] x-ray emission that was absent when a monatomic gas is irradiated under similar conditions. Absorption experiments demonstrated that nearly 100% of an intense laser pulse could be absorbed by a modest average density gas jet ($\sim 10^{19}\,\mathrm{cm}^{-3}$) within a few millimeters propagation length when clusters were present in the gas.[24,25] This laser absorption measurement indicated that many kiloelectron volts of energy per atom were being deposited in the clustering gas. The large absorption arises from the fact that the density within the clusters is high, nearly that of a solid, and can therefore exhibit the large absorption efficiency usually associated with solid targets.[4]

The mechanisms and dynamics of energy deposition by femtosecond pulses in individual clusters have also been examined by a number of groups. For example, it has been found that very high charge states are formed in the irradiation of high $Z$ noble gas clusters.[2,5,26] This high ionization of the cluster atoms is the result of a number of factors including enhanced tunnel ionization by charge resonant enhanced ionization, or so called "ionization ignition"[16] as well as traditional electron collisional ionization in the laser heated cluster.[4] Pump–probe and varying pulse-width experiments have been conducted which show that the clusters disassemble on a picosecond time scale.[12,13] Most interesting, however, has been the publication by a number of groups on the fast particles ejected from the explosions of these clusters upon intense irradiation. Photoelectron energy measurements indicated that multi-kiloelectron volt electrons are ejected from large (>1000 atom) Xe clusters.[27] Perhaps most remarkable has been the discovery that these large clusters, when irradiated at intensity above $10^{15}\,\mathrm{W/cm}^2$, also eject ions with substantial kinetic energy, a fact confirmed by a number of research groups world wide in recent years.[1,7,11,28]

This energetic cluster explosion is the result of rapid electron heating within the solid density cluster by the laser pulse. In large high $Z$ clusters, space charge forces confine the electrons to the charged ion sphere and a microplasma is created by field ionization. The laser can heat this electron cloud which then drives a rapid expansion of the cluster by the creation of a strong ambipolar electric field. In smaller clusters, or lower $Z$ clusters, such as hydrogen or deuterium, the laser field is strong enough to remove field ionized electrons directly from the cluster. In this case, the cluster explodes by the Coulomb repulsion of the closely spaced cluster ions. In either case, the accelerating fields in the cluster cause them to explode ejecting ions with substantial kinetic energy. It has been shown that this large release of kinetic energy in fast ions can be harnessed to drive nuclear fusion between deuterium ions if deuterium clusters are irradiated in a gas of sufficient average density to permit collision be-

[a]Present address: General Atomics, 10240 Flanders Court, San Diego, CA 92121.
[b]Present address: Department of Physics, San Jose State University, San Jose, CA.
[c]Present address: Center for Ultrafast Optical Science, University of Michigan, Ann Arbor, MI.

 

tween ions ejected from different clusters in the gas.[29] In these experiments, a high intensity, ultrafast laser pulse is focused into a gas jet of deuterium clusters, rapidly ionizing the inertially confined clusters before they can expand. These clusters subsequently explode, ejecting energetic ions. This process creates a plasma filament with a diameter roughly that of the laser focus ($\sim 100\ \mu$m) and a length comparable to the extent of the gas jet plume ($\sim 2$ mm). The fast deuterium ions ejected from the exploding clusters can then collide with ions ejected from other clusters in the plasma. If the ion energy is high enough (greater than a few tens of kiloelectron volts), nuclear fusion events can occur with high probability, releasing a characteristic 2.45 MeV neutron from the fusion reaction, $D+D \rightarrow He^3+n$.[30]

These phenomena represent an interesting possible source of pulsed, subnanosecond fast neutrons which could be used in neutron damage pump probe experiments.[31] Because of the need for much higher fusion yields to make this application possible, it is desirable to glean a detailed understanding of these phenomena. Previous work has shown some data on yield scaling with cluster size, along with an unexpected limit on neutron yield.[32] A better understanding of the factors affecting and limiting the fusion yield is needed to enable scaling of this source to much higher neutron fluences than demonstrated to date. In this paper we present a detailed experimental study of the exploding cluster physics, neutron yield, and laser energy deposition in the clustering gas jet. We find that the fusion neutron yield is strongly dependent on such factors as cluster size, laser focal geometry, and deuterium gas jet parameters. We also find that energy depletion of the laser pulse as it propagates through the absorbing cluster gas has a dramatic effect on neutron yield and is the ultimate limitation on the fusion yield in our experiments. Our results are consistent with a series of straightforward simulations.

## II. SIMPLE MODEL FOR EXPLODING DEUTERIUM CLUSTER FUSION YIELDS

To aid in interpreting the experimental results, we have developed some simple models. While modeling of all details of the interaction is extremely complex, we have found that straightforward scalings can be ascertained from some simple assumptions about the laser cluster interactions and fusion process in the deuterium gas.

To model the exploding cluster interaction, it is important to assume something about the shape of the ion spectrum resulting from the explosion of the clusters. The fusion cross section of DD fusion is very strongly dependent on ion energy, and only exhibits a significant value if the ions exhibit energies of a few to tens of kiloelectron volts. It has been shown by a number of groups that large, high $Z$, exploding clusters exhibit ion spectra that are similar to that of a hydrodynamically expanding gas.[11,33] This hydrodynamic explosion, however, is only appropriate when the ion charge of the cluster is very high and a large number of the electrons are retained in the cluster via space charge forces. Because deuterium cannot be ionized to high charge state it is likely that for reasonably sized deuterium clusters (thousands of atoms or less) the laser field will remove most or all of the electrons during the irradiation of the cluster. This results in a pure Coulomb explosion, akin to the Coulomb explosion of small molecules.

The intensity required to drive a pure Coulomb explosion is not easily calculated analytically; it depends on the dynamics of the driven electron cloud in the cluster. There are a few such simulations in the literature.[20] These simulations suggest that the cluster will be fully stripped of electrons by the laser field if the laser ponderomotive potential is comparable to or larger than the surface potential of the charged cluster. The energy of the Coulomb explosion will be maximized if the laser field satisfies this condition. If the ponderomotive potential is not high enough, the cluster will be stripped of some fraction of its electrons, raising the surface potential to a value near the ponderomotive potential.

The energy of the Coulomb explosion will be maximum if all electrons are stripped from the cluster on a time scale faster than that of the expansion of the cluster. Full removal of electrons prior to expansion leads to the largest stored potential energy in the cluster and the largest ion energies. This fact mandates that the rise time of the laser pulse (to the value of the stripping ponderomotive potential) be faster than some value. This characteristic explosion time can be estimated by calculating the time required for a charged cluster to expand to twice its initial radius, $a$. Integration of the motion of a charged deuterium cluster yields for this characteristic explosion time:

$$\tau_{\mathrm{Coul}} \approx 0.8 \sqrt{\frac{4\pi\epsilon_0 m_{\mathrm{D}}}{n_{\mathrm{D}} e^2}}, \tag{1}$$

where $m_{\mathrm{D}}$ is the mass of a deuteron and $n_{\mathrm{D}}$ is the density of deuterium atoms in the cluster, roughly $3\times 10^{22}\,\mathrm{cm}^{-3}$ for solid $D_2$. Note that $\tau_{\mathrm{Coul}}$ is independent of cluster radius and equals about 20 fs for deuterium clusters. This expansion time assumed an acceleration of a fully charged cluster and therefore represents a pessimistic limit on the necessary laser rise time. Nonetheless, Eq. (1) seems to suggest that our 35 fs pulses are marginally short enough to drive a Coulomb explosion at solid density.

If a Coulomb explosion is driven, and it can be assumed that all electrons are removed prior to any ion movement, the ion energy spectrum from a single exploding cluster, denoted $f_{\mathrm{sc}}(E)$, can be stated as (when normalized)

$$f_{\mathrm{sc}}(E) = \begin{cases} \frac{3}{2} E_{\mathrm{max}}^{-3/2} E^{1/2}, & E \leqslant E_{\mathrm{max}} \\ 0, & E > E_{\mathrm{max}} \end{cases}, \tag{2}$$

where $E_{\mathrm{max}}$ is the maximum energy of ions ejected and corresponds to those ions at the surface of the cluster. $E_{\mathrm{max}}$ is simply

$$E_{\mathrm{max}} = \frac{e^2 n_{\mathrm{D}} a^2}{3\epsilon_0}. \tag{3}$$

In deuterium clusters, $E_{\mathrm{max}}$ is about 2.5 keV for 5 nm clusters. Equation (3) illustrates that larger clusters are better for

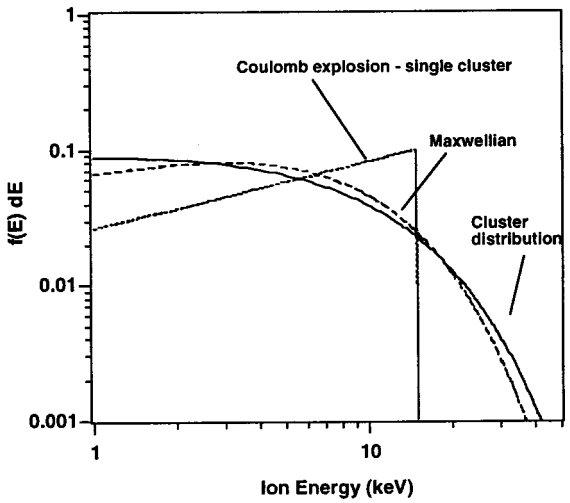


FIG. 1. Ion spectra for a cluster Coulomb explosion and a Maxwellian, each with a 9 keV average ion energy.

driving fusion because of the strong dependence of cross section with energy and the quadratic dependence of ion energy with cluster radius.

It should be noted that the single cluster ion energy distribution like that of Eq. (2) is not ideal for fusion. It is well known that in Maxwellian fusion plasmas of temperatures less than about 10 keV, the majority of the fusion occurs between the small fraction of ions in the hot tail of the Maxwellian, owing to the highly nonlinear increase in fusion cross section with ion energy in the 1–100 keV energy range. The Coulomb explosion ion spectrum has no hot tail, and, for equal average ion energies, has a dearth of hot ions as compared to a Maxwellian distribution. This is illustrated in Fig. 1 where spectra for a Coulomb explosion and a Maxwellian are compared, both with 9 keV average ion energy ($T_1=6$ keV for the Maxwellian and $E_{\max}=15$ keV for the Coulomb explosion).

In reality, the actual ion energy spectrum will be broadened by any distribution in cluster sizes in the target. In our experiments, the clusters are produced from a cooled gas jet, and it is well known that clusters formed from such jets exhibit a broad size distribution. This distribution in sizes, denoted $g(a)$, can be approximated as

$$g(a)=\beta a e^{-(a-a_0)^2/\delta^2}, \tag{4}$$

where $\beta$ is a normalization factor, and $\delta$ is a factor characterizing the width of the cluster size distribution. In this case, assuming that all clusters are completely ionized by the laser, the full ion energy distribution can be found by convolving the Coulomb explosion distribution of Eq. (2) and the cluster size distribution of Eq. (4):

$$f(E)=\int f_{\rm sc}(E)g(a)da=\frac{3\beta}{2}(e^2 n_{\rm D}/3\epsilon_0)^{-3/2}E^{1/2} \times \int_{\sqrt{3\epsilon_0 E/e^2 n_{\rm D}}}^{\infty} a^{-2}e^{-(a-a_0)^2/\delta^2}da. \tag{5}$$

Examples of this ion distribution with average ion energy of 9 keV are also shown in Fig. 1, where this corresponds to $a_0=6$ nm and $\delta=6$ nm This comparison shows that the convolved ion distribution closely approximates a Maxwellian.

The approximate ion distribution of Eq. (5) is not completely valid in modest laser intensity, If the laser intensity is not sufficient to fully strip the largest clusters, this will lead to a cutoff in ion spectrum at high energy. The exact nature of this cutoff requires detailed calculations of the laser cluster interactions. It is likely, however, that this effect can be approximated by cutting the ion spectrum at an ion energy near $U_p$, the laser peak ponderomotive potential. This is equivalent to saying that the laser strips the large clusters to potentials of $U_p$ instead of $E_{\max}$.

A calculation of the total fusion yield requires a calculation of all fast ion trajectories in the plasma. The ion mean free path for multi-kiloelectron volt deuterons in gas densities like that used in our experiments ($\sim 10^{19}\,{\rm cm}^{-3}$) is of the order of 2–5 mm. This distance is comparable to or longer than the characteristic sizes of the plasma filaments created in our experiment. Therefore, it is not appropriate to use a pure hydrodynamics calculation of the ion density and fusion burn evolution (though such simulations do provide important insight). Instead it is a good approximation to assume that all ions free steam from the interaction volume after the clusters explode and undergo fusion events as they traverse the plasma filament. In this case, the fusion yield will scale very roughly as

$$Y\sim n_{\rm gas}^2 l V\langle\sigma\rangle, \tag{6}$$

where $n_{\rm gas}$ is the average ion density in the gas jet target, $l$ is some characteristic escape distance (which is more or less the dimension of plasma filament), $V$ is the heated volume of gas, and $\langle\sigma\rangle$ is some appropriately weighted fusion cross section. This free streaming will occur on a time scale much longer than the explosions of the clusters. The clusters explode on a 100 fs time scale while the ions free stream across the plasma on a time scale $l/v_{\rm ion}\sim 100$ ps for ion velocities and plasma sizes of relevance in our experiments. Thus it is appropriate to think of the cluster explosion and subsequent fusion as decoupled events.

To calculate $\sigma$ in our simulations, we use the published scaling values of $\sigma(E_{\rm tot})$ for beam target fusion (ion hitting stationary ion) and setting

$$E_{\rm tot}=E_1+E_2+2\sqrt{E_1E_2}\cos\theta, \tag{7}$$

where $\theta$ is the angle of incidence between two ions. This is appropriate for nonrelativistic ions.

We have previously performed calculations of DD fusion yield in our experiment assuming that all ions free stream and that the heated plasma is a cylinder, with diameter given by that of the laser focal spot size. These results were published previously.[31] However, this simulation approach was found cumbersome. It is possible to make additional assumptions about the yield. If the cavitation of the plasma filament by escaping ions is ignored, the yield can be calculated from a relation like that of Eq. (6),

$$Y \approx \frac{n_{\mathrm{gas}}^2}{2} \int l(\mathbf{x},\mathbf{v}) dV \int\int\int \sigma(E_1,E_2,\theta) \times f(E_1) f(E_2) \frac{\sin\theta}{2} d\theta\, dE_1\, dE_2. \quad (8)$$

In the first integral, we find the average escape path length, a number which will depend on filament shape and aspect ratio. In the second integral, we find the weighted fusion cross section averaged over the ion energy distribution of test ions ($E_1$) and target ions ($E_2$). The factor of 1/2 accounts for double counting of ions. The fusion cross section is also averaged over all potential incident angles. We have numerically calculated the average ion escape trajectory distance by assuming plasma cylinders with initially uniform ion density and isotropic ion velocities and found that this value is equal to between 0.8 and 0.91 times the cylinder radius over a wide range of cylinder aspect ratios (radius/length between 3 and 50). Equation (8) leads to estimates for the yield that are within 40% of the full ion trajectory calculation of Ref. 31. Equation (8) allows an easy calculation of yield scaling with parameters such as cluster size and laser energy fluence. Details of such calculations are presented in Sec. IV.

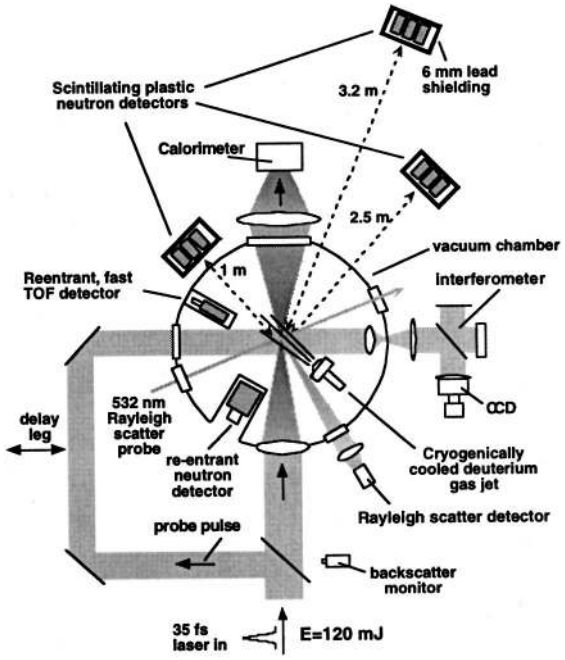


FIG. 2. Layout of our experiment with the suite of diagnostics.

## III. APPARATUS, $D_2$ CLUSTER TARGET, AND EXPERIMENTAL CHARACTERIZATION OF THE INTERACTION

The layout of our experiment with the suite of diagnostics is illustrated in Fig. 2. Our experiment utilized a 10 Hz, Ti:sapphire, chirped pulse amplification laser delivering 120 mJ of laser energy per pulse with 35 fs pulse width and wavelength of 820 nm. This laser was focused into the exit of a deuterium gas jet with an $f/12$ lens. We used a sonic gas jet with an orifice of 500 $\mu$m. This jet produced a broad plume as the gas expanded into the chamber. As the jet opened the pressure in the chamber would increase until the jet closed. Because the van der Waals forces between deuterium molecules are weak, the gas jet was cryogenically cooled by flowing cooled nitrogen or helium through a jacket surrounding the gas jet body. This encourages cluster formation. This jacket is similar to that described in Ref. 34. The cooled jet produced large clusters in the $D_2$ gas. We were able to cool the jet body to 100 K with liquid nitrogen, and to $<80$ K using liquid helium. This temperature was measured with a thermocouple mounted near the jet nozzle. We estimate that the actual gas temperature, particularly at thermocouple readings $<100$ K was lower than that registered.

The laser spot size within the gas jet varied from roughly 40 to 200 $\mu$m depending on the focal spot position, with respect to the gas jet nozzle. Consequently the peak laser intensity in vacuum (at 120 mJ) was between $2\times10^{16}$ and $4\times10^{17}$ W/cm$^2$. The laser propagation axis varied from 0.5 mm to roughly 2 mm below the output of the gas jet nozzle.

To estimate the deuterium cluster size in our gas jet, we conducted Rayleigh scattering measurements in the jet[35] by passing low energy ($<0.1$ mJ) 532 nm pulses from a frequency doubled, $Q$-switched Nd:YAG laser (pulse width 10 ns) through the plume of the gas jet. The Rayleigh scattered light was imaged 90° from the laser propagation axis (see Fig. 2). From the observed onset of Rayleigh scattering, we can determine the onset of large cluster formation in the jet.

Using independent measurements of the average gas density, estimates for the throughput and detection sensitivity, and the Rayleigh scatter cross section, we are able to estimate the average cluster size in the jet. Estimated cluster size as a function of temperature with a 70 atm backing pressure is illustrated in Fig. 3. This measurement, based on scattered light intensity, yields only a very rough estimate for the average cluster size. It is well known that clustering from an expanding jet results in clusters with a rather broad size distribution. Our scattering measurement gives us no direct information on this size spread. From Fig. 3 it is seen that we can roughly tune the average cluster size (by changing the gas temperature) from clusters of about 10 Å to over 100 Å.

The amount of laser energy absorbed in the gas jet was monitored in our experiments. To do this, we measured the transmitted laser energy collected within an $f/3$ cone (to collect all potentially refracted light from the $f/12$ cone) with a large aperture lens and calorimeter. We monitored backscattered light with a photodiode (very little was observed in these experiments). We also estimated scattered light using a charge coopted device (CCD) camera and collection lens monitoring light scattered 90° from the laser propagation direction perpendicular to the laser polarization direction (the direction of maximum Rayleigh scatter). Extrapolating into $4\pi$ we determined that the scattered light was negligible ($<1$ mJ).

The measured rise in energy absorption as the gas jet temperature is decreased is illustrated in Fig. 4. As can be seen from a comparison of Figs. 3 and 4, the absorption correlates quite closely to the growth of cluster diameter in the jet. This absorption difference cannot be explained by

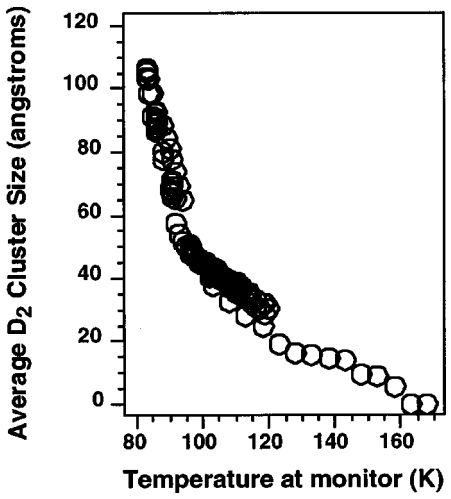


FIG. 3. Estimated cluster size as a function of temperature with a 70 atm backing pressure based on Rayleigh scatter data.

average density change alone and can only be explained by cluster formation. Over the range studied here, the gas density changed by approximately a factor of 2 as the jet is cooled from room temperature to 100 K, however, absorption increases by a factor of 20.

From interferometry measurements, described in Sec. V, we can make a reasonable estimate for the total energy deposited into deuterium ions based on absorption efficiency. This analysis[36] suggests that roughly 5 keV of energy are deposited per deuterium atom in the plasma. To ascertain the ion energies more accurately, we conducted ion energy measurement via ion time of flight (TOF). We installed a flight tube on the interaction chamber and detected ions ejected from the plasma with a microchannel plate detector. Flight distances of 1.4 and 2.5 m were utilized. The flight time of ions ejected from the plasma filament in the gas jet with respect to the laser irradiation time are measured. This technique is not an entirely accurate method of measuring ion energies given that the ions must traverse a small amount of unionized gas ($\sim$1 mm) prior to exiting the jet. We estimate that the mean free path of the kiloelectron volt ions in the gas is $\sim$1 cm, so the presence of unionized gas will have some affect on the measurement, particularly for the lower energy ions. The measurement is also complicated by space charge

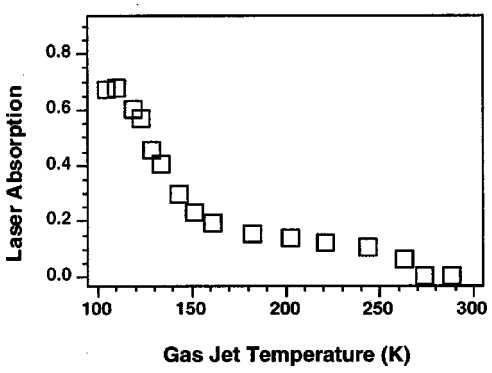


FIG. 4. Laser absorption as a function of gas jet reservoir temperature.

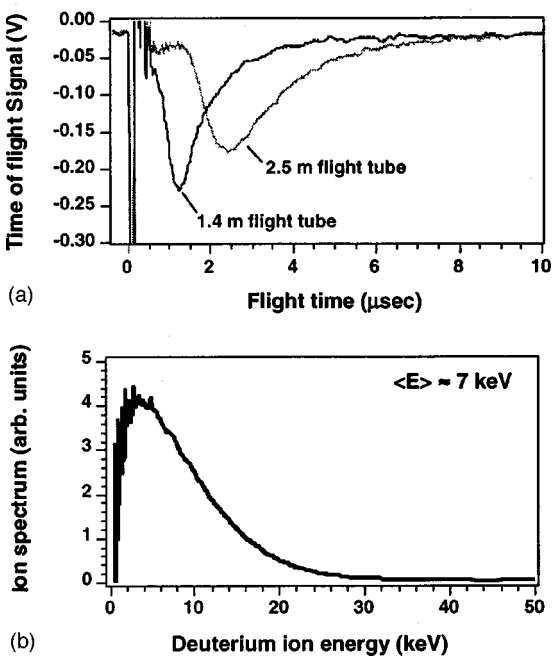


FIG. 5. (a) Time of flight ion spectra for two flight tube distances. (b) Energy spectrum derived from the 2.5 m flight data.

forces around the high density plasma filament. Nonetheless, this measurement yields a rough estimate for the ion energies produced by the exploding clusters. External magnets were installed on the flight tube to deflect low energy electrons.

TOF spectra for the two flight tube distances are illustrated in Fig. 5(a). An early time spike in the signal is observed from a flash of fast electrons and UV radiation from the plasma. The later time signal moves later with longer flight tube, confirming that the signal indeed arises from ions and not plasma radiation. An energy spectrum derived from the 2.5 m flight data is displayed in Fig. 5(b). This spectrum exhibits deuterons in a broad energy spectrum with energies extending out to nearly 30 keV. The average energy of ions found by averaging over this spectrum is 7 keV.

To detect the production of DD fusion neutrons in these experiments we employed arrays of neutron sensitive scintillators in various configurations. The layout of our detectors is shown in Fig. 2. Two classes of *n* TOF detectors were deployed. Detectors with large scintillator pieces were used to measure neutron yield. These detectors had high neutron detection efficiency (near unity). The initial detector of this kind was a grouping of three plastic scintillator cylinders, 12 cm in diameter and 10 cm long, coupled to two photomultiplier tubes (PMTs). These detectors were located outside the vacuum interaction chamber and were shielded with 6 mm of lead. Because of the small solid angle subtended, these were used in a single neutron counting mode. The second class of TOF detectors were thin scintillators closely coupled to PMTs, designed for high time resolution.[31] These detectors had subnanosecond response and could be used to examine the time structure of the neutron pulse.

With these neutron detectors we detected the presence of substantial numbers of 2.45 MeV neutrons when the gas was backed with cooled deuterium.[29] We observed no neutron

production with temperatures higher than 150 K, the temperature at which we no longer observe large cluster formation via Rayleigh scattering.

We were able to estimate the total fusion yield from the count rates on the large area neutron detectors and assuming near unity detection efficiency in the scintillators (an assumption that ensures the most pessimistic estimate for yield). The total yield of fusion neutrons varied with the laser and gas jet conditions. Detailed studies of the fusion yield will be presented in Sec. IV. However, we found that the highest yields attained tended to be around $\sim 2\times 10^4$ neutrons per shot.

Using the thin, high time resolution, neutron detectors we were able to measure the duration of the neutron pulse at several distances.[31] Since the neutron yield is nonlinearly dependent on the density [Eq. (6)], one would expect the fusion yield to only be significant before the plasma filament has had time to expand. The density of a multi-kiloelectron volt deuterium plasma filament with a diameter on the order of the laser focus will rapidly decrease to the point where fusion yield would be negligible. Our models showed that this time should be less than 1 ns. Figure 6 shows examples of the neutron pulse measured at several distances. The best fit was calculated using a Gaussian pulse convolved with the time response of the detector. The increasing pulse width with distance comes about from Doppler broadening. Extrapolating to zero distance, one finds that initial pulse is $\sim$500 ps.[31] How rapidly the pulse broadens as one moves away from the source gives information on the temperature of the plasma.[37] From this, the mean ion temperature is estimated to be about 8 keV, which is similar to the ion TOF data previously discussed.

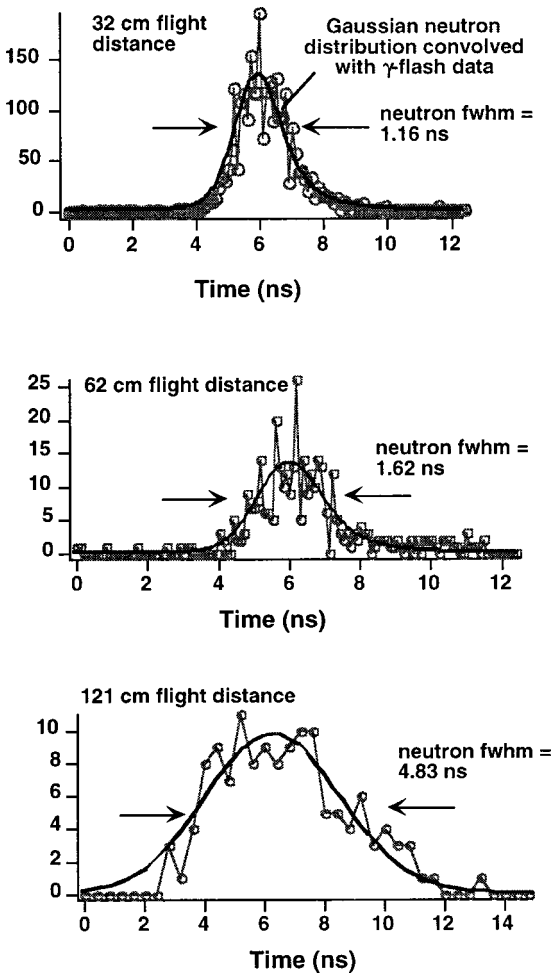


FIG. 6. Neutron pulse width data from the 12×12 cm detectors at a variety of distances.

## IV. EXPERIMENTAL MEASUREMENTS OF FUSION YIELD SCALING

To derive a greater understanding of the nature of the fusion neutron production in this interaction, we have examined the fusion yield as a function of a wider range of laser parameters. These studies were conducted in a number of ways. The primary diagnostic for measuring the fusion yield was an additional large plastic scintillator detector, placed near the plasma in a reentrant flange to subtend a large solid angle. It subtended a solid angle of 0.3 sr and was placed 20 cm from the deuterium plasma. Because the time-of-flight data indicate that there is no noticeable x-ray flash and that virtually all of the detected particles are neutrons, we can obtain a shot by shot measure of the fusion yield from the PMT signal. The detection efficiency was calibrated against the other neutron TOF detectors operating in single particle detection mode. We also calibrated the yield by measuring the average pulse height produced when single neutrons struck the detector. Both methods yielded nearly equal values for the yield calibration.

As discussed in Sec. II, the Coulomb explosion model of the fast deuterium ion production predicts that a strong dependence of fusion yield should exist with increasing average cluster size. The data of Sec. III indicate that we can control the average cluster sizes from about 10 to 100 Å by varying the gas jet reservoir temperature. The fusion yield measured through this technique as a function of cluster size is illustrated in Fig. 7. Each data point represents the integration of five laser shots. The shot to shot spread in the data was substantial ($>$50%) owing to the counting statistics from the detection of a limited number ($<$100) of neutrons per shot. This plot represents two data sets, plotted as circles and squares. The circle data points were taken with the laser focus approximately 1 mm before the center of the gas jet nozzle. This focal point was chosen to optimize the yield at a jet temperature of 100 K. The square points were taken with the laser focus slightly further away from the nozzle center. As expected, the fusion yield rises rapidly from about 100 neutrons per shot with average cluster size of 30 Å and peaks at around $10^4$ *n*/shot when the average size in the jet reaches 55 Å. At higher cluster sizes, corresponding to colder gas jet temperature, the yield rolls over and falls off. Using Eq. (8), we have calculated the expected fusion yield as a function of cluster size and compared these predictions with the data. These calculations are shown in Fig. 7 as solid lines. We use the ion energy distributions of Eq. (5) and have varied the width of the cluster size distribution, assuming that the width parameter, $\delta$, was equal to a constant factor times the average

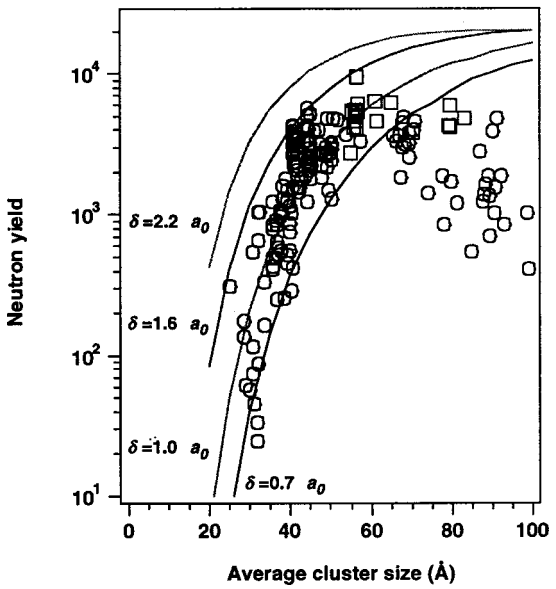


FIG. 7. Measured and calculated fusion yield as a function of cluster size.

cluster diameter. Cluster size distribution widths of 0.7, 1, 1.6, and 2.2 times the average cluster diameter are plotted. This comparison shows that the data, up to the peak in yield at 55 Å, exhibit a yield increase that follows the calculations quite well, with the best fit being for the calculation conducted with cluster size distribution width equal to the cluster size. This comparison appears to indicate that the trend predicted by the Coulomb explosion model is correct.

The model calculations indicate that the fusion yield will continue to grow as the average cluster size increases beyond 55 Å. The rollover seen at higher average cluster size seen in the data is inconsistent with this trend. Clearly, our simple model will break down when the cluster sizes become large enough that the laser field can no longer completely strip the clusters, driving the Coulomb explosion. The rollover we observed, however, is likely the result of more complicated effects. The simple model of Sec. II does not account for the fact that the real experiment consists of a laser pulse propagating into a spatially broad clustering medium. This can lead to refraction and absorption of the laser prior to its reaching the center of the gas jet plume. We have examined these effects in detail through interferometric imaging of the laser plasma in the jet. These experiments will be described and analyzed in Sec. V.

To gain a greater insight into the fusion production we have also examined yield as a function of a variety of other parameters. The measured fusion yield as a function of gas jet backing pressure is illustrated in Fig. 8. Here the gas jet was held at a temperature of 100 K, the point of peak yield seen in Fig. 7. The incident laser energy was 120 mJ. No neutrons are observed at backing pressure below 23 atm. The yield then increases rapidly at pressure above 23 atm. This correlates to the point at which large clusters are observed in the Rayleigh scattering. These data were taken with the laser focus (measured in vacuum) 1.3 mm before the center of the gas jet.

An important trend observed in our experiments was that

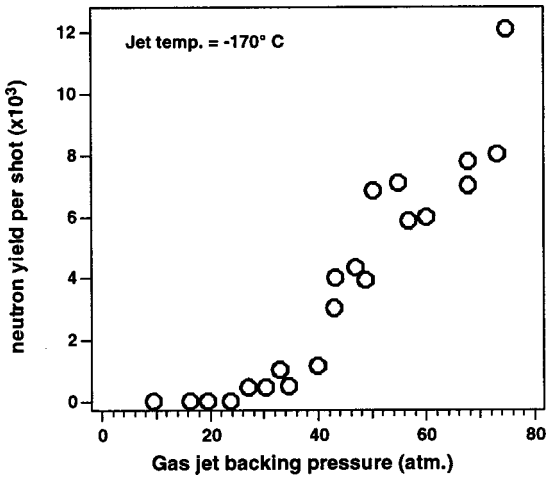


FIG. 8. Measured fusion yield as a function of gas jet backing pressure.

the fusion yield was very sensitive to the position of the focus with respect to the center of the gas jet. We found that the optimum yield occurred when the laser was focused before the center of the gas jet. This effect is illustrated in Fig. 9, which shows fusion yield measured as a function of laser focal position with respect to the center of the gas jet for a variety of different gas jet backing pressures. In these data, the laser energy was 50 mJ and the gas jet temperature was 100 K. First, we see that, at the highest backing pressure, the yield peaks when the laser is focused ~0.75 mm before the gas jet, even through the highest gas density is at jet center. The yield has dropped by ~20% when the laser is focused right at the center of the gas jet.

Also important to note is the fact that the peak yield position moves closer to the gas jet center as the backing pressure of the jet is increased. For the lower pressures (<40 atm) though the yield is quite low, it peaks when the laser focus is far from the jet center. The strong dependence of optimal position with gas jet pressure suggests that this effect is the result of some variation in the laser propagation through the gas. It should be noted that the observed trend is

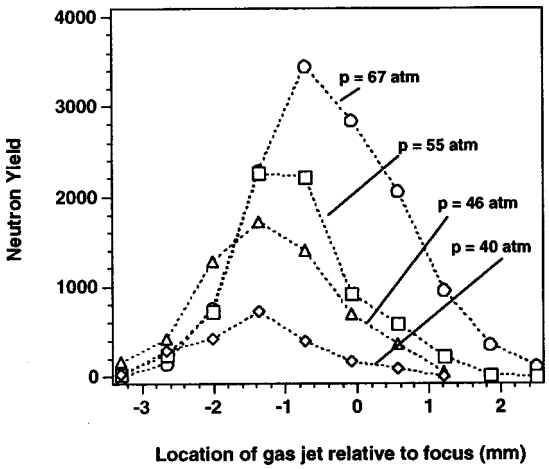


FIG. 9. Fusion yield measured as a function of laser focal position with respect to the center of the gas jet for a variety of different gas jet backing pressures.

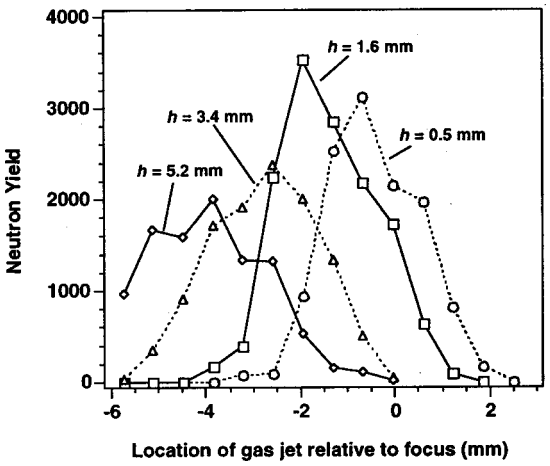


FIG. 10. Fusion yield measured as a function of laser focal position with respect to the center of the gas jet for a variety of different separations between the jet and the laser propagation axis.

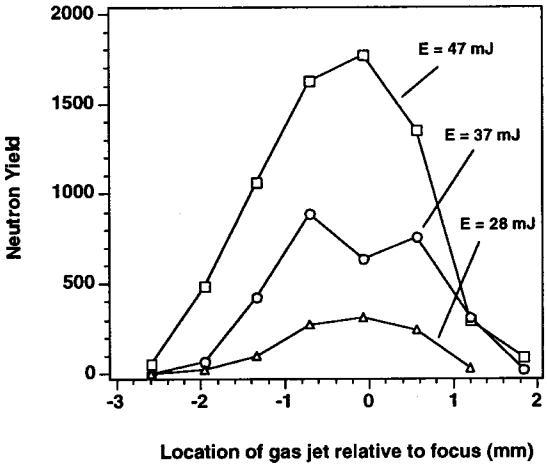


FIG. 11. Laser focal $z$ scans at different incident laser energies.

counter to a simple explanation based on ionization induced refraction. Refraction will tend to increase the laser size as it passes into the jet, so focusing before the jet center would not counteract this effect.

Similar behavior is observed when the distance between the gas jet nozzle and the laser propagation axis are varied. Data illustrating this are shown in Fig. 10. Because of the diverging cone of gas, increasing this nozzle–laser distance will decrease the average density and will broaden the spatial extent of the gas through which the laser propagates. We see that the yield peak with focal position variation shifts toward the center of the jet as the distance between the nozzle and laser axis decreases.

Data showing laser focal $z$ scans at different incident laser energies are shown in Fig. 11. The optimal focal position, as the laser energy is varied, does not appear to move. The peak yield more or less rests at the same point as the laser energy is decreased.

From these data we can determine the yield scaling as a function of energy. The simple model described in Sec. II suggests that the yield should increase at least as fast as the 3/2 power of the laser energy. This scaling results if the laser intensity is kept constant and the spot size is allowed to increase as the laser energy grows. Thus, constant intensity yields constant ion energy, so the growth in yield results from a growth in heated volume (linear with energy) and the growth in mean ion transit distance, shown to be near the focal spot radius in Sec. II for a cylindrical plasma. Since this focal spot radius will increase as the square root of energy, this implies a total yield scaling of laser energy to the 1.5 power. Of course this estimate is not valid when the laser focal spot approaches the same dimension as the deposition length. However, in our experiment the focal spot was always $<200$ $\mu$m, which is at least an order of magnitude smaller than the 2 mm deposition length. Nonetheless, this estimate likely represents a worse case scaling, since greater yield may be derived if the intensity is increased (greater cluster sizes can be fully stripped, for a more energetic Coulomb explosion) or the laser penetrates more effectively into the gas jet plume.

The measured yield scaling with laser energy is illustrated in Fig. 12. We observe a yield scaling from 25 to 120 mJ at $E^{2.2}$, substantially faster than our simplistic yield scaling estimate. The origin of this fast yield scaling can be, in fact, attributed to the way in which more energetic laser pulses propagate into the jet. This will be considered in Sec V.

We have also examined the falloff of neutron yield as we change the intensity though a lengthening of the laser pulse. This pulse lengthening was achieved by chirping the pulse through a detuning of the pulse compressor. Yield as a function of the laser pulse width is illustrated in Fig. 13 (with all other parameters kept constant). Instead of the rapid fall seen when the laser energy is decreased (Fig. 12) the yield falls off slowly as the pulse is broadened from 30 to 300 fs (a drop in intensity by a factor of 10 results in a yield decrease of only a factor of 3.5). The yield falls off more rapidly at longer pulse widths. This weak initial scaling of yield with pulse width of course suggests that the strong scaling seen in Fig. 12 is not attributed simply to laser intensity, but instead is a result of a decrease in laser fluence.

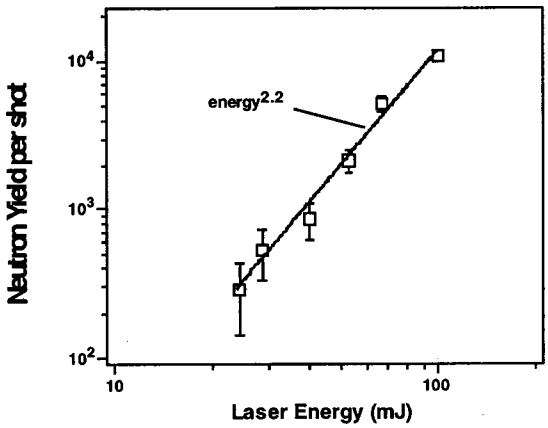


FIG. 12. Measured neutron yield scaling as a function of laser energy.

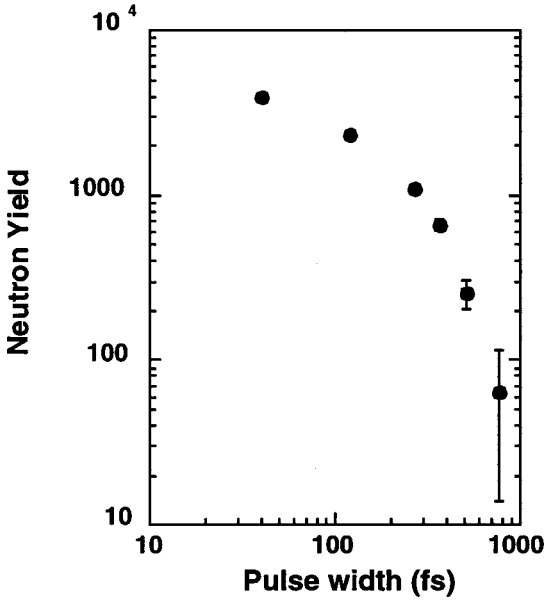


FIG. 13. Measured yield as a function of the laser pulse width.

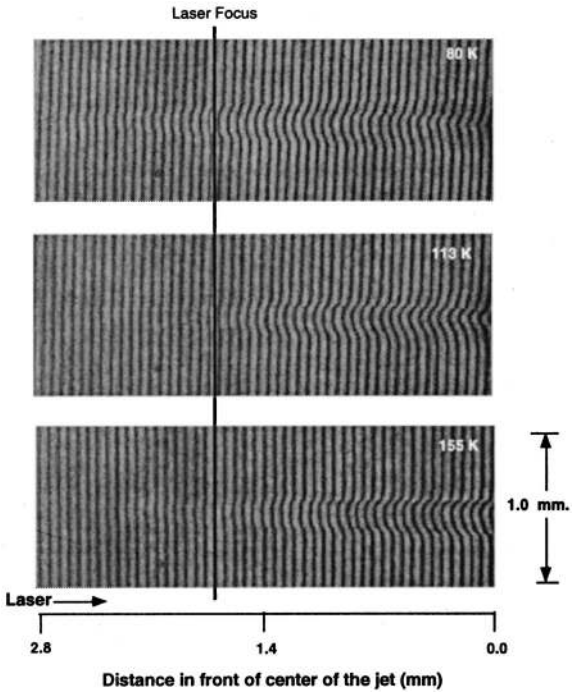


FIG. 14. Interferograms along the laser propagation axis approximately 20 ps after the laser ionizes the gas for three measured gas jet temperatures 80, 113, and 155 K.

## V. LASER PROPAGATION IN THE DEUTERIUM JET

As mentioned in Sec. IV, while we expect the neutron yield to increase as the jet temperature falls and the cluster size increases, this trend does not hold beyond a certain jet temperature. In order to study these effects we performed time resolved interferometry on the laser plasma. The diagnostic is illustrated in Fig. 2. A small portion of the laser beam is split off and sent across the target transverse to main laser beam. The probe pulse is then analyzed in a Michelson interferometer. By varying the delay of the probe pulse we can watch the evolution of the expanding laser plasma. The resulting interferograms can be Abel inverted to find the electron density of the plasma. This ionization information can then be used to discern where the laser is depositing energy. An example of such raw interferometric data is illustrated in Fig. 14, in which the images are recorded with the probe delayed only 20 ps after the ionizing laser traverses the medium, a time well before any hydrodynamic motion of the ions occur. The fringe deviation indicates the area and shape of the ionized deuterium ''cigar-shaped'' filament.

We imaged the plasma at different jet stagnation temperatures to understand how the laser propagation is affected by the gas temperature, and hence cluster size. Figure 14 shows interferograms along the laser propagation axis at different gas temperature. The three images are for 80, 113, and 155 K. The ionized region appears to move upstream of the laser focus (to the left in the images) as the jet temperature decreases. Figure 15 shows electron density along the center of the laser axis as determined from the Abel inversion of the interferograms in Fig. 14. The maximum measured electron density is $\sim 1.5-2.0\times 10^{19}\,\mathrm{cm}^{-3}$. This small variation indicates that the observed gas temperature effects on yield are not likely the result of changing average density. The electron density rises as the pulse propagates toward the center of the jet, illustrating the rise in gas density toward the center of the plume. However, the electron density rolls over and decreases prior to the center of the jet plume, for the data collected at the lower temperature. At lower temperature this rollover indicates that the laser does not penetrate effectively to the center of the jet. As we move to higher temperatures the laser can clearly propagate further into the gas plume. A higher electron density is reached further before the jet, and

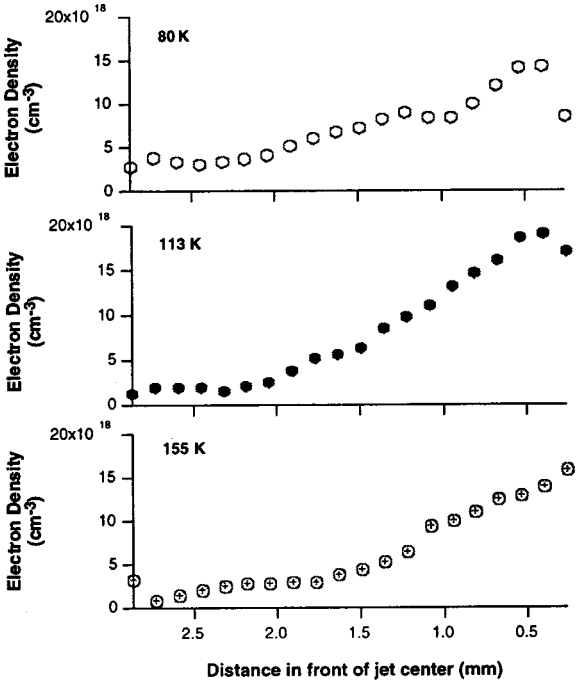


FIG. 15. Deconvolved electron density along the center of the laser axis determined from the interferograms of Fig. 14.

in the case of the highest temperature, the electron density does not roll over. This likely results from there being less energy absorbed per atom in the smaller clusters, and the laser pulse can travel further before the energy is depleted.

The neutron yields in the previous cases were $\sim 7 \times 10^3$ at 80 K, $4 \times 10^2$ at 113 K, and 0 at 155 K. This is remarkable, with over an order of magnitude increase in neutron yield from 113 to 80 K despite the fact that the average ion density is higher at $T = 113$ K. Clearly the laser energy must be absorbed over a smaller number of ions, creating a higher effective ion temperature, at the colder jet temperature.

More information about the laser energy absorption and ion temperature can be found in looking at the velocity of the blast wave formed as the plasma expands radially. The velocity of a cylindrically symmetric Tayler–Sedov blast wave will scale roughly as $(E_l/\rho_0)^{1/4}$, where $E_l$ is the energy deposited per unit length and $\rho_0$ is the average gas density.[38] Thus, faster blast waves indicate larger energy deposition per atom is the gas. While it is difficult to compare maximum energy deposition between two different images because of the weak quarter power scaling, we can derive some information about where the laser deposits its energy along its propagation path by examining where the later time (few nanoseconds) blast wave expands with greatest velocity.

This is illustrated by data shown in Fig. 16. These images are taken 4 ns after the laser pulse ionizes the gas, a time after the blast wave has developed and expanded over a distance many times the initial plasma filament diameter. We see that for 80 K the largest radius, and hence greatest energy per ion deposition, occurs at the point where the laser reaches best focus. The laser will exhibit the highest intensity here and hence be able to strip the electrons from the larger clusters and produce the highest energy ions. This in turn produces the highest neutron yield for the largest clusters even though the maximum energy deposited at other temperatures occurs at higher densities.

These data indicate that an important factor in achieving higher neutron yields is to arrange the laser focal position to deposit the laser energy to the highest density region of the jet before the pulse is depleted. To illustrate this point we altered the spatial characteristics of the jet plume by altering the timing between the jet opening time and the point at which the laser fires. Two shots with different initial jet opening times are shown in Fig. 17. The bottom image was taken with the gas jet fired 500 $\mu$s earlier than the upper image. The total jet opening time was 800 $\mu$s. When the jet is opened earlier there is more time for the flow to develop and the size of the plume is larger. This increased plume size (of the later opening time, bottom image) leads to laser energy absorption much further upstream than when the jet is opened right before the laser arrives (upper image). The deconvolved axial electron density plots illustrate this, as shown in Fig. 18. When the jet is opened early, the electron density peaks further in front of the center of the jet. The energy is depleted prior to the laser focus. The effect of this is shown in Fig. 19 where the blast waves (at 4 ns) of these situations are reproduced. The blast waves show that the energy is absorbed much further forward in the jet and far in front of the laser focus when the jet plume is allowed to expand before the laser arrives (lower image). This means, of course, that the laser energy is absorbed at lower laser intensity in this case. Only small clusters can be fully stripped of electrons and the average explosion energies will be lessened. Indeed, the early opening jet (larger plume, bottom image in Fig. 19) yielded $\sim 2 \times 10^3$ neutrons while the later opening jet (more tightly confined plume) produced $\sim 8 \times 10^3$ neutrons.

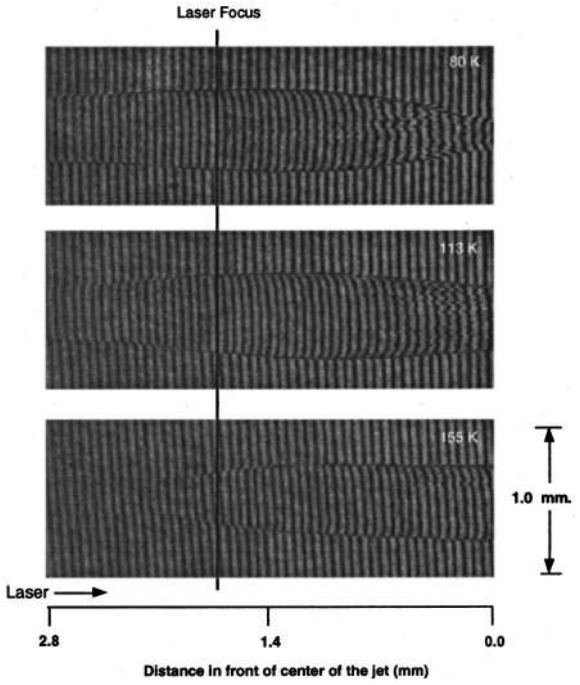


FIG. 16. Interferograms at three different gas jet temperatures taken 4 ns after the laser irradiates the jet showing the extent of the resulting blast wave.

These energy depletion issues in the laser propagation can easily explain the scaling data seen in Fig. 10 when the distance from jet nozzle to laser axis is varied. Figure 20

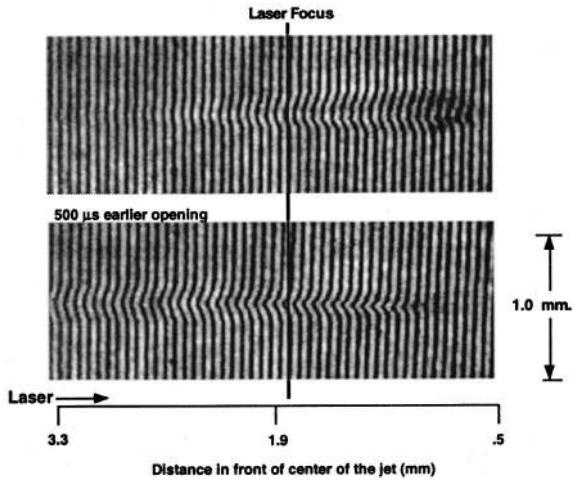


FIG. 17. Interferograms (at 20 ps) of shots with different initial jet opening times. The upper image shows the plasma created when the laser arrives within close ($\sim 100$ $\mu$s) to the initial jet opening. The bottom image is taken when the laser irradiates the jet well after ($>500$ $\mu$s) the jet opens.

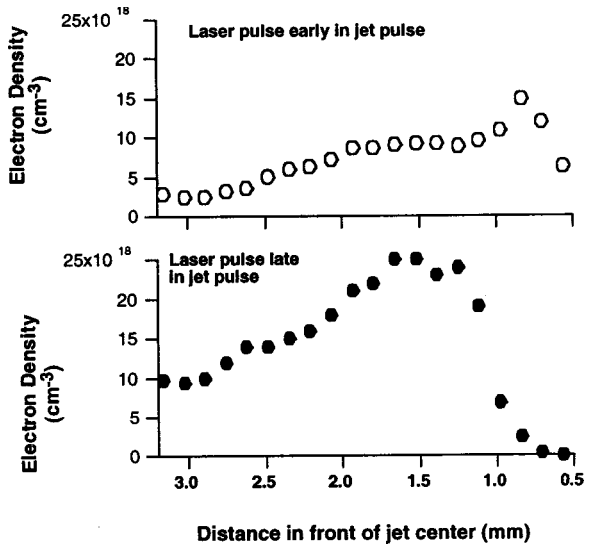


FIG. 18. Deconvolved axial electron density plots derived from the two interferograms in Fig. 17.

shows images of the plasma when the laser and gas jet are separated by three different distances. Clearly the laser energy is absorbed further upstream as the distance is increased and the effective gas density gradient scale length is lengthened. As previously, images of blast waves (at 3 ns), shown in Fig. 21, confirm that the location of the large energy absorption with respect to the jet center changes with nozzle–axis separation. It appears as if the maximum energy absorption occurs very close to best focus at separation of 1.6 mm while it occurs before focus at 3.4 mm and after focus for 0.5 mm. The neutron yield in these experiments was $2.5\times10^3$ for 0.5 mm separation, $3.5\times10^3$ for 1.6 mm (best match of laser focus and energy deposition point) and $1\times10^3$ for 3.4 mm. Once again we see that the maximum neutron yield occurs when the point of highest energy absorption coincides with best laser focus.

The gas jet backing pressure scaling of neutron yield presented in Sec. IV was somewhat unexpected. The higher

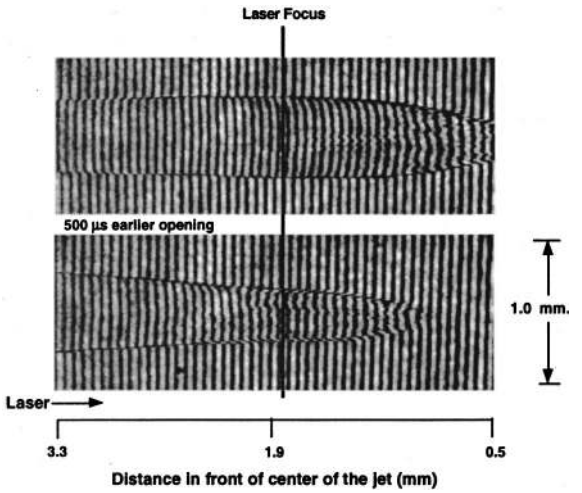


FIG. 19. Blast wave profiles determined 4 ns after irradiation of the two jet opening times shown in Fig. 17.

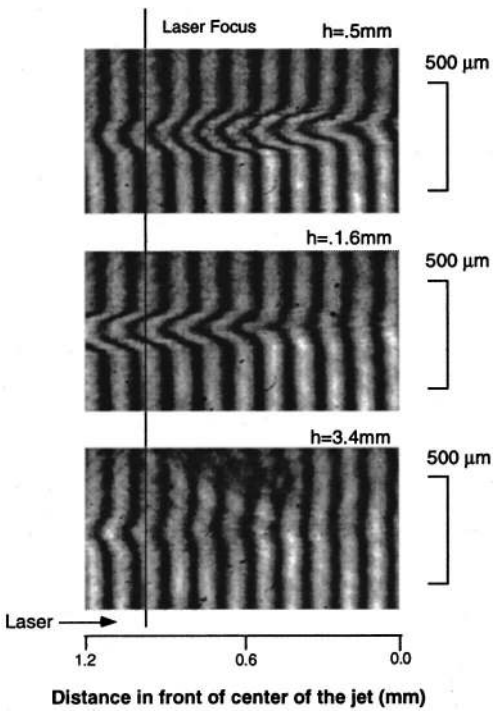


FIG. 20. Interferometric images (at 20 ps) of the plasma when the laser propagation axis and gas jet are separated by three different distances.

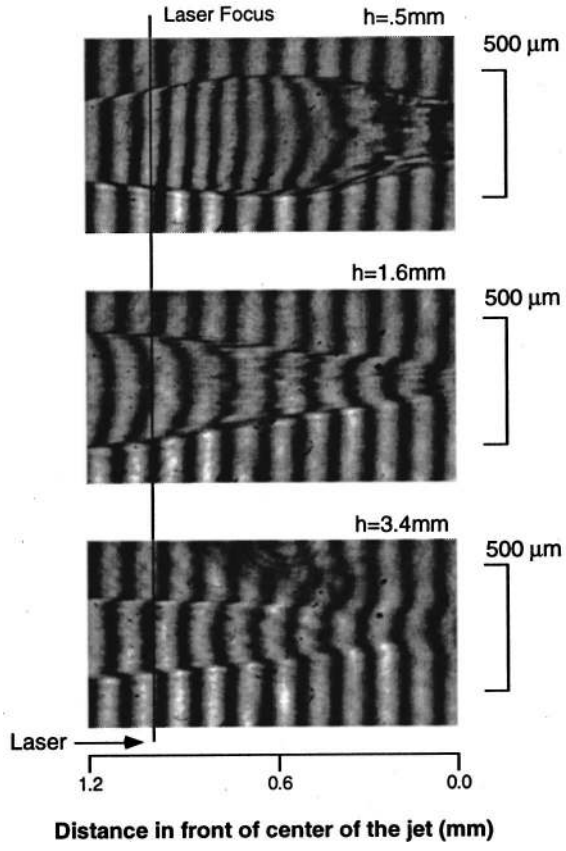


FIG. 21. Blast wave profiles (at 3 ns) of the three gas jet-laser axis separations used in Fig. 20.

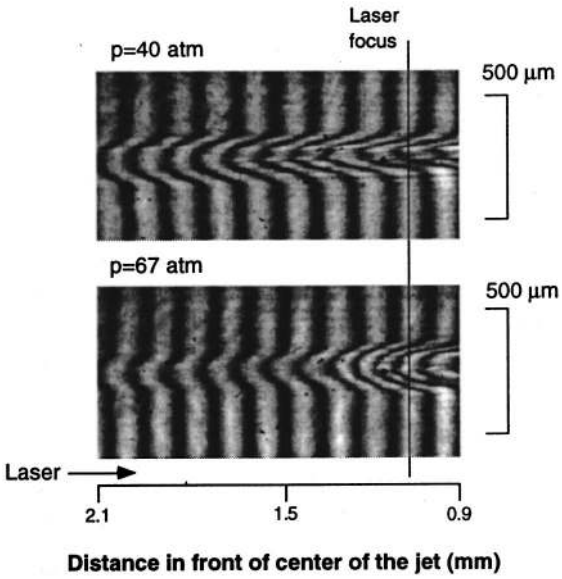


FIG. 22. Interferograms (at 20 ps) of the plasma at two different gas jet backing pressures.

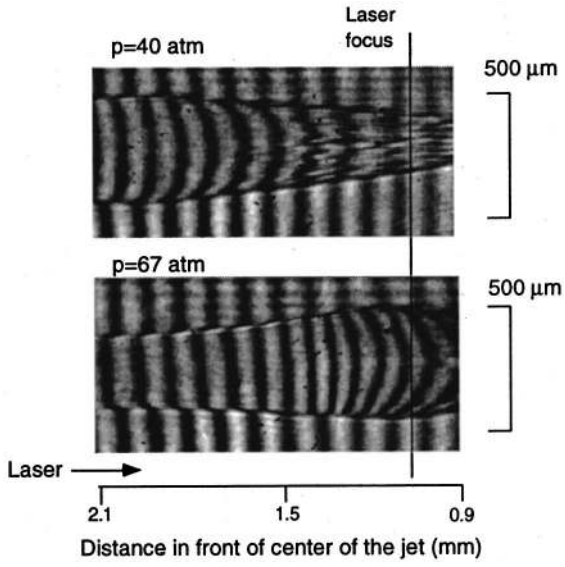


FIG. 23. Blast wave profiles (at 3 ns) of the plasma at two different gas jet backing pressures used in Fig. 22.

densities at higher pressures should lead to more absorption further in front of the jet. Intuitively this would lead to the optimal jet position being further behind the focus, so that the best focus can be placed where the laser energy is being absorbed. This would be similar to what was observed in the height scaling as the separation is increased. The opposite trend is observed in the jet pressure scaling, however, with the optimal position at 67 atm resting closer to the focus than at 40 atm (Fig. 11). The interferograms in Fig. 22 clearly show the reason for this observed trend. The plasma is forming further forward at 40 atm than at 67 atm. Examination of the electron density shows that, even though the pressure is higher at 67 atm, the density is lower out in front of the jet plume center than with 40 atm backing, showing that the plume is better collimated at higher backing pressure. There is less gas along the path toward the jet center at higher backing pressure and the laser can penetrate further. This effect is likely a consequence of changing jet dynamics as the pressure increases. Finally, this supposition is confirmed in the blast waves after 3 ns (Fig. 23). For data from the blast wave for the 67 atm case, absorption occurs at best focus, while it occurs well ahead of best focus at 40 atm. The neutron yields for these cases were $4\times10^3$ at 67 atm and $7\times10^2$ for 40 atm.

## VI. CONCLUSION

In this paper we have presented an extended study of the scaling of fusion from the irradiation of a gas of deuterium clusters with an intense 35 fs laser pulse. The various measured scalings indicate that a Coulomb explosion model of the ion energy is a good description of the ion explosion. The consequence of this is that larger clusters will clearly be advantageous in producing faster ions (and higher fusion yields) if high enough laser intensity can be achieved to fully strip the clusters. It is clear from our measurements that, when a sonic nozzle like that utilized in our experiments is employed, the diffuse cluster plume can lead to substantial depletion of the laser during its propagation to the jet center. This has an important effect on the fusion yield. This initial battery of research now points to a number of improvements to increase neutron yield in this experiment, namely using well collimated plumes of large deuterium clusters and higher energy femtosecond lasers.

## ACKNOWLEDGMENTS

We would like to acknowledge the technical assistance of V. Tsai, G. Anderson, and R. Shuttlesworth.

[1] J. Purnell, E. M. Snyder, S. Wei, and A. W. Castleman, Jr., Chem. Phys. Lett. **229**, 333 (1994).
[2] A. McPherson, B. D. Thompson, A. B. Borisov, K. Boyer, and C. K. Rhodes, Nature (London) **370**, 631 (1994).
[3] T. Ditmire, T. Donnelly, R. W. Falcone, and M. D. Perry, Phys. Rev. Lett. **75**, 3122 (1995).
[4] T. Ditmire, T. Donnelly, A. M. Rubenchik, R. W. Falcone, and M. D. Perry, Phys. Rev. A **53**, 3379 (1996).
[5] E. M. Snyder, S. A. Buzza, and A. W. Castleman, Phys. Rev. Lett. **77**, 3347 (1996).
[6] D. A. Card, D. E. Folmer, S. Sato, S. A. Buzza, and A. W. Castleman, J. Phys. Chem. A **101**, 3417 (1997).
[7] T. Ditmire, J. W. G. Tisch, E. Springate, M. B. Mason, N. Hay, R. A. Smith, J. Marangos, and M. H. R. Hutchinson, Nature (London) **386**, 54 (1997).
[8] S. Dobosz, M. Lezius, M. Schmidt, P. Meynadier, M. Perdrix, D. Normand, J. P. Rozet, and D. Vernhet, Phys. Rev. A **56**, R2526 (1997).
[9] M. Lezius, S. Dobosz, D. Normand, and M. Schmidt, J. Phys. B **30**, L251 (1997).
[10] S. Dobosz, M. Schmidt, M. Perdrix *et al.*, JETP Lett. **68**, 485 (1998).
[11] M. Lezius, S. Dobosz, D. Normand, and M. Schmidt, Phys. Rev. Lett. **80**, 261 (1998).
[12] J. Zweiback, T. Ditmire, and M. D. Perry, Phys. Rev. A **59**, R3166 (1999).
[13] L. Koller, M. Schumacher, J. Kohn, S. Teuber, J. Tiggesbaumker, and K. H. Meiwes-Broer, Phys. Rev. Lett. **82**, 3783 (1999).
[14] J. W. G. Tisch, N. Hay, E. Springate, E. T. Gumbrell, M. H. R. Hutchinson, and J. P. Marangos, Phys. Rev. A **60**, 3076 (1999).
[15] E. Parra, I. Alexeev, J. Fan, K. Y. Kim, S. J. McNaught, and H. M. Milchberg, Phys. Rev. E **62**, R5931 (2000).
[16] C. RosePetruck, K. J. Schafer, K. R. Wilson, and C. P. J. Barty, Phys. Rev. A **55**, 1182 (1997).

[17]M. Brewczyk, C. W. Clark, M. Lewenstein, and K. Rzazewski, Phys. Rev. Lett. **80**, 1857 (1998).
[18]L. Poth and A. W. Castleman, J. Phys. Chem. A **102**, 4075 (1998).
[19]M. Brewczyk and K. Rzazewski, Phys. Rev. A **60**, 2285 (1999).
[20]I. Last and J. Jortner, Phys. Rev. A **60**, 2215 (1999).
[21]V. P. Krainov and M. B. Smirnov, Usp. Fiz. Nauk **170**, 969 (2000).
[22]V. P. Krainov and M. B. Smirnov, JETP **92**, 626 (2001).
[23]M. B. Smirnov and V. P. Krainov, Phys. Scr. **63**, 157 (2001).
[24]T. Ditmire, R. A. Smith, J. W. G. Tisch, and M. H. R. Hutchinson, Phys. Rev. Lett. **78**, 3121 (1997).
[25]K. Kondo, A. B. Borisov, C. Jordan, A. McPherson, W. A. Schroeder, K. Boyer, and C. K. Rhodes, J. Phys. B **30**, 2707 (1997).
[26]T. Ditmire, J. W. G. Tisch, E. Springate, M. B. Mason, N. Hay, J. Marangos, and M. H. R. Hutchinson, Phys. Rev. Lett. **78**, 2732 (1997).
[27]Y. L. Shao, T. Ditmire, J. W. G. Tisch, E. Springate, J. Marangos, and M. H. R. Hutchinson, Phys. Rev. Lett. **77**, 3343 (1996).
[28]S. Dobosz, M. Schmidt, M. Perdrix *et al.*, JETP **88**, 1122 (1999).
[29]T. Ditmire, J. Zweiback, V. P. Yanovsky, T. E. Cowan, G. Hays, and K. B. Wharton, Nature (London) **398**, 489 (1999).
[30]E. Teller, *Fusion* (Academic, New York, 1981), pp. 25 and 26.
[31]J. Zweiback, T. E. Cowan, R. A. Smith, J. H. Hartley, R. Howell, C. A. Steinke, G. Hays, K. B. Wharton, J. K. Crane, and T. Ditimire, Phys. Rev. Lett. **85**, 3640 (2000).
[32]J. Zweiback, R. A. Smith, T. E. Cowan, G. Hays, K. B. Wharton, V. P Yanovsky, and T. Ditmire, Phys. Rev. Lett. **84**, 2634 (2000).
[33]T. Ditmire, E. Springate, J. W. G. Tisch, Y. L. Shao, M. B. Mason, N. Hay, J. Marangos, and M. H. R. Hutchinson, Phys. Rev. A **57**, 369 (1998).
[34]R. A. Smith, T. Ditmire, and J. W. G. Tisch, Rev. Sci. Instrum. **69**, 3798 (1998).
[35]R. Klingelhöfer and H. O. Moser, J. Appl. Phys. **43**, 4575 (1972).
[36]T. Ditmire *et al.*, Phys. Plasmas **7**, 1993 (2000).
[37]D. R. Slaughter, Rev. Sci. Instrum. **60**, 552 (1989).
[38]A. Cavaliere and A. Messina, Astrophys. J. **209**, 424 (1976).